Heliyon 10 (2024) e26071

Contents lists available at ScienceDirect

Heliyon

journal homepage: www.cell.com/heliyon

Research article

3D printed polycaprolactone/β-tricalcium phosphate/carbon nanotube composite – Physical properties and biocompatibility

Yuelei Wang [a], Chenjing Liu [b], Tao Song [c], Zhenlu Cao [c], Ting Wang [a,*]

[a] The Affiliated Hospital of Qingdao University, Shinan District, Qingdao, 266005, China
[b] Yantai Yuhuangding Hospital, Zhifu District, Yantai, Shandong, 264008, China
[c] Shunde Hospital of Southern Medical University, Shunde District, Foshan, Guangdong, 528000, China

ARTICLE INFO

Keywords:
3D printing
Carbon nanotube
Elastic modulus
Porosity
Cytocompatibility

ABSTRACT

Three-dimensional (3D) printing is a bio-fabrication technique used to process tissue-engineered scaffolds for bone repair and remodeling. Polycaprolactone (PCL)/β-tricalcium phosphate (TCP) has been used as a base and osteoconductive biomaterial for bone tissue engineering in the past decades. The current study reveals the fabrication of a polycaprolactone (PCL)/β-tricalcium phosphate (TCP) scaffold by incorporating carbon nanotubes (CNT) via 3D printing. The physical properties and cytocompatibility of a new type of tissue engineering composite from polycaprolactone/β-tri-calcium phosphate/carbon nanotubes were investigated, and it was an absorbable scaffold prepared via furnace deposition 3D printing technology. The scaffold was designed with CAD software, and the composite material was fabricated via 3D printing. The printed composite material was tested for mechanical strength, scanning electron microscope (SEM) analysis, porosity calculation, systemic toxicity test, hemolysis rate determination, and effect on the proliferation of rat adipose-derived stem cells cultured in vitro. A composite scaffold with a length of 15 mm, width of 10 mm, and height of 5 mm was manufactured through CAD software drawing and 3D printing technology. Scanning electron microscopy measurements and analysis of the internal pore size of the stent are appropriate; the pores are interconnected, and the mechanical strength matches the strength of human cancellous bone. The calculated porosity of the stent was >60%, non-toxic, and non-hemolytic. The proliferation activity of the ADSC co-cultured with different scaffold materials was as follows: polycaprolactone/β-tricalcium phosphate/0.2% carbon nanotube scaffolds > polycaprolactone/β-tricalcium phosphate/0.1% carbon nanotube scaffolds > polycaprolactone/β-tricalcium phosphate/0.3% carbon nanotube scaffolds > polycaprolactone/β-tricalcium phosphate scaffolds ($P < 0.05$). The results showed that polycaprolactone/β-tricalcium phosphate/0.2% carbon nanotube scaffolds promoted the adhesion and proliferation of ADSC. The combination of 3D printing technology and CAD software can be used to print personalized composite stents, which have the characteristics of repeatability, high precision, and low cost. Through 3D printing technology, combining a variety of materials with each other can provide the greatest advantages of materials. The waste of resources was avoided. The prepared polycaprolactone/β-tri-calcium phosphate/0.2% carbon nanotube scaffold has a good pore structure and mechanical properties that mimic human cancellous bone, is non-toxic and non-hemolytic, and is effective in promoting ADSC proliferation in vitro. Given this correspondence, 3D printed scaffold shows good biocompatibility and strength, and the fabrication

* Corresponding author.
E-mail address: wting_2023@outlook.com (T. Wang).

https://doi.org/10.1016/j.heliyon.2024.e26071
Received 28 August 2023; Received in revised form 30 January 2024; Accepted 7 February 2024
Available online 20 February 2024
2405-8440/© 2024 The Authors. Published by Elsevier Ltd. This is an open access article under the CC BY-NC-ND license (http://creativecommons.org/licenses/by-nc-nd/4.0/).

method provides a proof of concept for developing scaffolds for bone tissue engineering applications.

1. Introduction

In the past, bone defects caused by trauma, osteonecrosis, and tumor lesions were treated with autologous bone, allogeneic bone, or xenon bone transplantation. However, autologous bone has limitations in clinical application owing to difficulties in obtaining materials, donor site infection, and chronic pain [1]. At the same time, allogeneic and xenogeneic bone have risks such as weak bone induction, disease transmission and immune rejection [2,3]. Therefore, the search for an ideal bone graft has become key to the treatment of bone defects. Bone tissue engineering is a novel treatment that has gained interest in the treatment of hard tissue repair/restore/remodeling. Scaffolds used in tissue engineering are greatly influenced by two main factors: the materials used and fabrication methods [4]. Optimized scaffolds are produced through a novel material processing technique, known as additive manufacturing or 3D printing. Polycaprolactone (PCL) is one of the most widely used polymers for preparing scaffolds, particularly for 3D printing [4].

The scaffold has the capacity to mimic native tissue in the design of tissue engineering templates for the regeneration of hard and soft tissues from their defects. These fibrous scaffolds have the potential to enhance the mechanical strength of the scaffold and provide structural support for cell development. Furthermore, cells cultured on fibrous scaffolds tend to retain their phenotypic shape because of the morphology of the scaffolds, which is similar to that of the extracellular matrix found in nature. PCL can be used to fabricate microfibers and nanofibers for the fabrication of tissue engineering scaffolds. One area of potential improvement in scaffold behavior in osteochondral applications is the incorporation of micro- and nanofibers into the scaffolds [5]. With the continuous progress in tissue engineering technology, the research and development of various bone tissue engineering scaffolds [6,7] that can induce tissue regeneration provides a new idea for the exploration of bone grafts. In addition, the emergence of 3D printing technology has significantly improved the accuracy and repeatability of the support. Polycaprolactone (PCL) is a biological scaffold material with thermal stability, biodegradability, and plasticity [8]; however, it cannot meet clinical needs because of its poor biological activity, slow degradation, poor mechanical strength, and hydrophobicity, which are not suitable for osteoblast adhesion [9–11]. β-Tricalcium phosphate (β-tricalcium phosphate, β-TCP) has bone conductivity, absorbability, and degradability, and calcium ions produced during degradation can promote osteogenic differentiation of stem cells [12–14], there is uncontrollable brittleness [15].

PCL is a semi-crystalline hydrophobic polymer with a low melting point, good mechanical qualities, good biocompatibility, and no antigenic effects. Its degradation product was non-toxic. Furthermore, PCL exhibits good adhesion to various substrates and mechanical compatibility with numerous biomaterials. However, this does not result in the formation of a new bone at the defect site. Combining PCL with biomaterials to promote ossification is a method of improving and enhancing it. These biomaterials include various calcium phosphate compounds and natural and synthetic ceramics such as hydroxyapatite [4].

Melt-extrusion 3D printing was used to fabricate degradable scaffolds as tissue precursors. Varying ratios of the natural biopolymer chitosan or bioceramic β-tricalcium phosphate (TCP) were blended with PCL to fabricate support scaffolds for human bone marrow-derived mesenchymal stem cell growth. Varying ratios of natural biopolymer, chitosan, bioceramic, and β-tricalcium phosphate (TCP) were blended with PCL to fabricate support scaffolds with a three-dimensional architecture for human bone marrow-derived mesenchymal stem cell (hBMSC) growth. Scaffold morphology and microarchitecture promote cell growth for the potential use of 3D melt-extruded PCL-based composite scaffolds in regenerative and bone repair applications [16].

Traditional approaches based on scaffolds and microengineering rarely produce tissue structures with the appropriate biomimetic properties. In principle, 3D bioprinting provides an unprecedented opportunity to precisely control the composition, spatial distribution, and precise composition of cells and biological materials, thereby achieving a good structure and composition of tissues and biological materials, thus achieving reproduction and personalization of organs. Advances in 3D bioengineering technology and bioinks are relevant for production processes. We focus on the use of this technology in the creation of biomimetic structures for many tissues and organs, including the blood vessels, heart, liver, and cartilage [17]. Polycaprolactone (PCL) is widely used in tissue engineering owing to its low melting temperature, good processability, biodegradability, biocompatibility, mechanical resistance, and relatively low cost. Advances in additive manufacturing (AM) technology over the past decade have reduced processing times, eliminated material waste, and facilitated the production of customized PCL products [18].

The incorporation of Carbon nanotubes (CNT) into scaffolds results in excellent mechanical, chemical, and structural stability, as well as high electrical, thermal, and bioactivity properties [19]. In addition, the reinforcement of tissue-engineered scaffolds with CNTs increases the wettability of the scaffolds [19]. The incorporation of β-TCP with a PCL scaffold increases the performance of the scaffold in terms of strength, hydrophilicity [206], and cell growth [20,21]. Further, the addition of β-TCP in the PLA scaffolds increases the degradation rate of 3D printed scaffolds and also osteo-conductivity, which is beneficial for the application of composite scaffolds in the field of tissue engineering [22].

Carbon nanotubes (CNTs) have superior mechanical strength and are considered as good composite reinforcement [23]. Therefore, in this study, the melt deposition modeling (FDM) technology in 3D printing was implemented to add CNTs to PCL in different proportions/β- Composite absorbable material PCL prepared in TCP/β- TCP/CNT, and investigated its physical properties and biocompatibility.

2. Materials and methods

2.1. Design

Material and animal comparative experiment. The number of replicates used in each characterization methods are three and the data taken from these studies are averaged"

2.2. Time and place

The experiment was completed in Qingdao University from June 2019 to June 2020.

2.3. Materials

Experimental animal: Wistar rats, 10 week old female (Beijing weitonglihua Experimental Animal Technology Co., Ltd., license No.: scxk (Jing 2016–0006), Certificate No.: 1100111911053155).

Main experimental materials, instruments and reagents: 3D printer and supporting CAD software (motor assisted microsyringe rapid prototyping system, Shanghai fuqifan electromechanical Co., Ltd., China); Universal material testing machine (model z020, Zwick/Roell, Germany); Scanning electron microscope (jsm-7500f field emission scanning electron microscope, Japan); Low temperature plasma hydrogen peroxide sterilizer (model: sq-d Shandong Xinhua Medical Instrument Co., Ltd., China); Tin melting furnace (working temperature 550 °C, power 0.15kw, Ruirui hardware factory, Caitang Town, Chao'an county, Guangdong, China); Super clean workbench (model sw-cj-1c, cleanliness class 100, Shanghai Precision Instrument Co., Ltd., China); cutting machine (model yj-510cnc, Yueqing Deshun Machinery Co., Ltd., China); enzyme labeling instrument (model elx 800, bio-tek Baote company); inverted phase contrast microscope (CKX41, Olympus company); constant temperature water bath box (model: hh-50l anqing Jiejia Instrument Equipment Co., Ltd., China); desktop centrifuge (Shanghai Anting Flying Pigeon company); ion sputtering instrument (model: jfc-1600, Japan Electronics Co., Ltd., Japan) DMEM/F12 medium: purchased from Solarbio; fetal bovine serum: purchased from GIBCO; glutamine: purchased from Solarbio; non essential amino acids: purchased from Solarbio; penicillin/Streptomycin Solution (P/s 100x): 10000 units/ml salt solution of penicillin and 10000 μl/ml streptomycin, purchased from Solarbio company; trypsin: purchased from GIBCO company; type I collagenase: purchased from sigma company; CCK-8 test kit: purchased from Solarbio company; PBS (1x): purchased from hyclone company; anhydrous ethanol: purchased from Sinopharm Chemical Reagent Co., Ltd.

2.4. 3D printing PCL/β- TCP and PCL/β- preparation of TCP/CNT composite scaffold

According to previous studies β- When tricalcium phosphate is added in more than a certain proportion (more than 30%), the nozzle will be blocked and the material cannot be discharged. Therefore, the most common proportion method is selected in this study, namely polycaprolactone: β- Composite scaffolds [24–26] were made based on tricalcium phosphate in the ratio of 8:2 β- TCP and CNT are combined in different proportions as per the composition in Table 1. PCL required for weighing and β- TCP, put it into a beaker, stirred and mixed with a glass rod, and then put it into a tin melting furnace for heating. The temperature was maintained at 230 °C, stirred with a metal rod, add the required CNT for many times, and melted for many times to ensure uniform mixing to avoid any inhomogeneity in the components. The required graphics are designed with CAD software, and then the path program is exported with the software of 3D printer. The printer parameters was fixed as per the requirements of fiber diameter 500 μm, aperture 360 μm and layer height 5 mm. The well mixed composite materials were added into the melting barrel for printing. After 3D printing, it was allowed for 1 min. After the sample is well cooled, sterilized it in a low-temperature plasma hydrogen peroxide sterilizer for 90 min, and sealed the composites for further characterization. Fig. 1 shows the scaffold model to be 3D printed for developing tissue engineering scaffold.

2.4.1. Composite support characterization

2.4.1.1. Microscopic morphology observation. The 4 different groups of scaffolds were divided and cut the specimen to an appropriate size. The samples were fixed on the copper plate with conductive adhesive, and spray gold on the scaffolds under vacuum with JFC-1600 ion sputtering instrument. The surface morphology, pore structure and pore size of composite scaffolds were observed under electron microscope acceleration voltage of 10 kV.

Table 1
Preparation and composition of composite scaffold.

Bracket group	compound material (wt%)		
	PCL	TCP	CNT
PCL/β-TCP	80	20	0
PCL/β-TCP/0.1%CNT	80	19.9	0.1
PCL/β-TCP/0.2%CNT	80	18.8	0.2
PCL/β-TCP/0.3%CNT	80	19.7	0.3

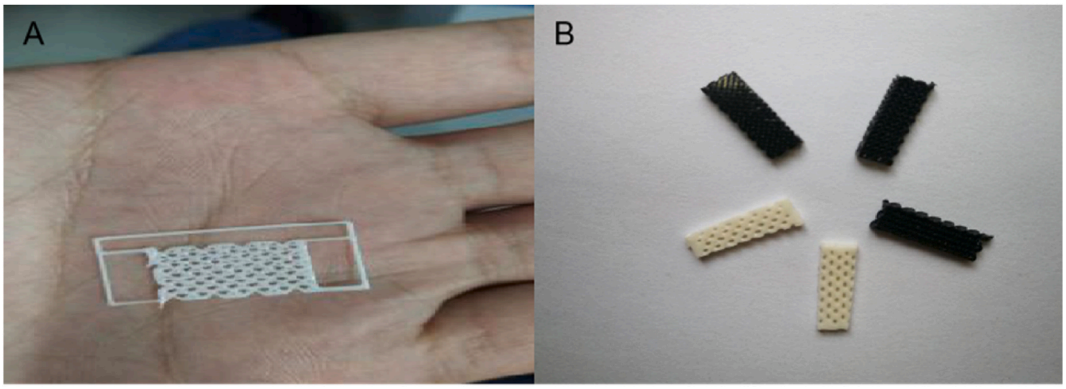

Fig. 1. A shows the model processing function of CAD software. The model is layered to obtain a single-layer two-dimensional plane support. B shows length: width: height = 15 × 10 × 5 mm PCL with different ratio of CNT/β- TCP/CNT support.

2.4.1.2. Mechanical property test. The 4 groups of specimen were taken and, tested their elastic modulus with universal material testing machine, and used for compression test. The compression modulus is 2 mm/min. The whole compression process was carried out at the rate of 5 mm/min. The stress of each group of materials were measured at the compression rate of 20%, 40%, 60% and 80%, and measured for 5 samples in each group. The stress-strain curve was drawn through the obtained data and combined with Hooke's law formula $\sigma = E \cdot \varepsilon$ (σ: Stress, unit: MPa; E is elastic modulus, unit: MPa; ε: Strain (unit:%) calculated the elastic modulus of the corresponding specimen and the compressive strength at the corresponding compression rate. The protocol for mechanical strength of the 3D printed scaffold was as follows. This method was performed as per ISO 17162. Compression testing was performed using a Zwick/Roell Z005 material testing apparatus, which employed a 2.5 KN load cell to monitor force variations and crosshead displacement. To identify variations of 3 N in applied force and the displacement of the crosshead from its initial position, a 2.5 kN load cell was utilized. Using hydraulic controls, the load cell was manually moved to a point around 2 mm above the test specimen (standard compression modulus 2 mm/min). From here, software was used to start a preload process that brought the crosshead into contact with the specimen. Software was used to start the preload step and manually adjust the load cell. The specimen failed at a crosshead speed of 5 mm/min, within 10–30 s. There was a 1.5 KN top force limit, and end-of-test controls were used to show when the specimen failed.

2.4.1.3. Porosity measurement. The 4 groups of support samples was taken, poured an appropriate amount of absolute ethanol into a sealed measuring cylinder, which is calculated as V1; The sample holder was put into the measuring cylinder containing absolute ethanol, and read out the volume V2 when there is no bubble; Take out the support in the cylinder and read out the volume V3 of residual absolute ethanol in the measuring cylinder; That is, V1–V3 is the pore volume of the sample, and v2-v1 is the volume of the sample support material; Using Archimedes principle, P=(V1–V3)/(v2-v1) × 100% measure the porosity of the prepared scaffold, where p is the porosity of the composite scaffold; Measure 5 samples in each group and calculate the average porosity.

2.4.2. Preparation of composite scaffold material extract

According to the method in the national standard biological evaluation of medical devices Part 12: sample preparation and reference samples, each group of composite scaffolds after sterilization are prepared into sample material extraction solution, which is added into the extraction medium normal saline and culture medium containing 10% fetal bovine serum according to the sample surface area/extraction medium of 3 cm^2/ml. Put it into a 37 °C incubator and let it stand for 72 h to obtain the scaffold extract and the scaffold extract cell culture solution. Filter the extract with a 0.22 μm bacterial filter and store it at a low temperature of 4 °C for standby.

2.4.3. Systemic toxicity test

According to previous studies, CNT has certain toxicity [21], so we set the extract prepared by the 0.3% CNT group scaffold with the highest CNT content as the experimental group. 0.9% normal saline was used as the blank control group. Six 12 week old rats, weighing 370 ± 2.5G, were randomly divided into experimental group and control group, with 3 rats in each group (as shown in Table 2). Each animal in the experimental group was intraperitoneally injected with 4 ml of extract, and each animal in the control group was intraperitoneally injected with 4 ml of 0.9% normal saline. After injection, the general physiological conditions of rats such as activity, mental status, diet, sleep and defecation were observed within 72 h. Record the occurrence of poisoning and death. One week later, the

Table 2
Grouping of toxicity test.

Grouping	Intraperitoneal injection	Injection volume (ml)	Quantity (pieces)
Experience group	Composite scaffold extract	4	3
Control group	0.9% normal saline	4	3

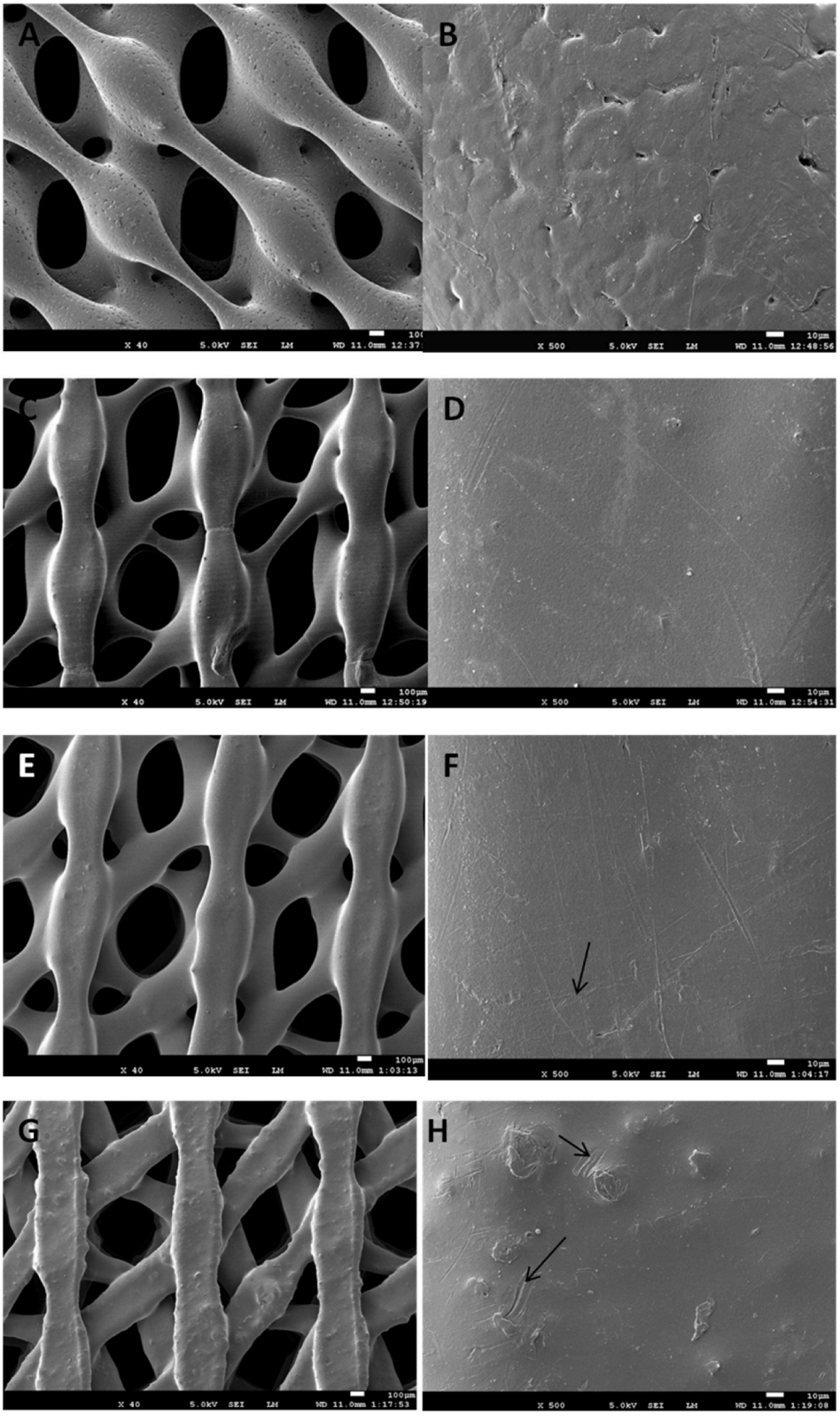

(caption on next page)

Fig. 2. Shows the microstructure of composite scaffolds with different CNT ratios under electron microscope × 40 × 500)-Note: as shown in Figure B, the local magnification is 500 times of the micrograph of Fig A, and white dots can be seen β- Tricalcium phosphate is evenly distributed in polycaprolactone; D shows its local magnification of 500X micrograph of C, with β- Tricalcium phosphate decreased without obvious β- TCP particles and CNT tubular structure, the support surface is smooth and flat; F shows its local magnification of 500X micrograph E, with β- Tricalcium phosphate decreased and the content of carbon nanotubes increased, resulting in tubular carbon nanotubes (indicated by the arrow); H shows its local magnification of 500X G micrograph due to β- The content of tricalcium phosphate is further reduced, the nozzle resistance is reduced, the scaffold fiber becomes flat, the content of carbon nanotubes increases, granular protrusions on the scaffold surface (Fig. g), and a large number of carbon nanotubes with tubular structure appear (arrow in Fig. h). Figure A shows the PCL/β-TCL 3D Printed Scaffold at 100 μm and Figure C, E, G are PCL/β-TCL/CNT with different proportions scaffold at 100 μm.

above experimental rats were killed. The liver and kidney organs of the rats were paraffin sectioned and stained with H&E. The liver and kidney tissues were observed for cell poisoning under the microscope.

2.4.4. Hemolysis test

According to the national standard biological evaluation of medical devices Part 4: selection of interaction test with blood, a 12 week old rat was randomly captured and anesthetized by intra-peritoneal injection of 10% chloral hydrate at the ratio of 0.1 ml/10 g. After anesthesia, 5 ml syringe was used to collect blood from the heart, 2 ml blood was extracted and put into heparin tube, and 2.5 ml 0.9% normal saline was added to make the diluted rat anticoagulant. The experiment was divided into positive control group (distilled water group), negative control group (normal saline group) and experimental group (containing 0% CNT, 0.1% CNT, 0.2% CNT and 0.3% CNT). Six test tubes were taken to mark the group number and the same amount of 10 ml distilled water, 0.9% normal saline and extracts of each group were added respectively. Put all test tubes into a 37 °C constant temperature water bath and preheat for 30min. Add 0.2 ml of diluted rat anticoagulant into each test tube, and then put it into a 37 °C water bath for 50min. After incubation, 750 g was centrifuged for 5 min. Absorb the supernatant and place it on a 96 well plate with 100 μl per well, and set 3 multiple holes in each group. The absorbance of each group was measured at the wavelength of 545 nm of the microplate reader, and each group was measured three times. Calculate the hemolysis rate of each group. The hemolysis rate is expressed in P, the mean absorbance of the negative control group is expressed in B, the mean absorbance of the experimental group is expressed in a (A1, 2, 3), and the mean absorbance of the positive control group is expressed in C. according to formula P = (a-b)/(C–B) × The hemolysis rate was calculated at 100%. According to the national standard, if the hemolysis rate of biomaterial is ≤ 5%, the biomaterial meets the hemolysis requirements of the evaluation standard. If the hemolysis rate is >5%, it indicates that the biomaterial has hemolysis and does not meet the hemolysis requirements of the evaluation standard.

2.4.5. Extraction, passage and culture of rat adipose mesenchymal stem cells in vitro

One healthy rat was killed by decapitation after anesthesia. The inguinal area was cleaned and prepared for skin disinfection. The bilateral inguinal adipose tissue was taken by laparotomy and put into the Petri dish. It was washed repeatedly with PBS solution containing 2 wt % penicillin streptomycin for 3 times, and the fascia and blood vessels visible to the naked eye were removed with ophthalmic scissors. The remaining adipose tissue was cut into chyle shape and transferred into a centrifuge tube, Add 2 times the volume of 1% type I collagenase, fully mix it, and then digest it in a 37 °C constant temperature water bath. Shake and mix it every 5 min. After the adipose tissue is fully digested, add an equal volume of culture medium containing 10% fetal bovine serum to terminate the digestion. Centrifuge at 1200 R/min for 5 min, discard the supernatant, resuspend the cells with the culture medium containing 10% fetal bovine serum, and filter with a 200 mesh cell sieve, Prepare a uniform cell suspension, inoculate it in a 6 cm^2 Petri dish, culture it in an incubator with a volume fraction of 5% CO_2 and 95% humidity at 37 °C, change the solution after 48 h, and then change the solution every 24 h. When the cells grow to 90% confluence under the microscope, remove the culture medium, wash with PBS twice, add 1 ml of 0.25% trypsin (including EDTA), shake the culture dish slightly to make the liquid level fully cover the bottom of the dish, observe the morphological changes of the cells under the microscope, when most of the adherent cells are completely suspended, add 2 ml of culture medium containing 10% Fetal Bovine Serum (FBS) to stop digestion, and blow it fully and repeatedly to form a single cell suspension, Transfer into a 15 ml centrifuge tube at 1200 R/min and centrifuge for 5min. After cell counting, the cells were resuspended and cultured until the third generation.

2.4.6. The culture of rat adipose mesenchymal stem cells on the scaffolds

The proliferation rate of rat adipose mesenchymal stem cells was evaluated by CCK method. The third generation adipose mesenchymal stem cells were digested with 0.25% trypsin and centrifuged to make cell suspension. After cell counting, they were inoculated according to the inoculation amount of 5 × 104 cells per well. After being cultured in the incubator for 24 h, the following different culture media were replaced according to the requirements of experimental grouping: negative control group (normal culture medium), experimental group (soaking culture medium of different scaffolds), The blank control group (only culture medium, no cells) was set. The amount of liquid added to each well was 100 μl, 9 wells in each group, and the liquid was changed every other day. Take out 96 well plates on the 2nd, 4th and 6th days of culture, add 10 μl CCK-8 solution to each group, incubate in the incubator for 3 h, take out the samples, measure the absorbance of each group at 450 nm with an enzyme labeling instrument, and according to the formula, the relative cell proliferation rate (OD) = [a (experimental group) - A (blank group)]/[a (negative group) - A (blank group)] × The OD value of cells in each group was 100%, so as to evaluate the cytotoxicity of scaffolds.

2.4.7. Statistical analysis

All data in the experiment were analysed by SPSS 17.0 statistical software. Unless otherwise specified, each sample in the triplicate was measured and the mean of the data were expressed by X ± s (Mean ± SD). If it conforms to the normal distribution, the LSD test of one-way ANOVA is used for multi group mean multiple comparison. The difference was significant ($P < 0.05$).

3. Results

3.1. Morphology observation of composite scaffolds under electron microscope

The PCL was observed by SEM/β- TCP and PCL/β- The TCP/CNT composite support is shown in Fig. 2 below. The surface morphology of the scaffold shows the network matrix formed by multi-layer extrusion material deposition. The morphology of the scaffold and the pore distribution on the whole scaffold are uniform, rather than the non crosslinked scaffold. It can be seen from the electron microscope that the pores of each layer of the scaffold are interconnected and nearly oval. These pores play an important role in the transportation of nutrients, oxygen and waste. The pore size less than 100 μm is not conducive to chondrogenic differentiation, and the cells with too large pore size lose support and are not conducive to growth [27,28]. The internal pore diameter and fiber diameter of the composite support were measured by origin 8 mapping software (as shown in Fig. 4), PCL/β- The pore diameter of TCP stent group was 366.1 ± 57.47 μm, PCL/β- The pore diameter of TCP/0.1% CNT stent group was 389.5 ± 66.71 μm, PCL/β- The pore diameter of TCP/0.2% CNT stent group was 396.2 ± 73.23 μm, PCL/β- The pore diameter of TCP/0.3% CNT stent group was 378.4 ± 48.53 μm, and the corresponding stent fiber diameters were 351 ± 43.21 μm, 377.4 ± 52.44 μm, 374 ± 50.45 μm and 368.8 ± 49.73 μm, respectively. It has been found that human mesenchymal stem cells (MSCs) in scaffolds with pore size of 250–450 μm have high cell activity [29,30]. After 1000 times magnification, it was observed that the CNT is in a tubular structure, β- TCP has a white powdery structure, and the above two substances are evenly distributed in PCL polymer, as shown in Fig. 3.

3.2. Analysis of porosity and mechanical properties of composite support

According to Archimedes principle, the porosity of composite scaffolds with various ratios was calculated by ethanol replacement method. In terms of porosity (Table 3), the porosity of the four composite scaffolds is 60.42 ± 0.21% - 65.07 ± 0.10%, which is in line with the porosity of bone tissue engineering scaffolds reported in the literature (35%–75%), which is conducive to cell adhesion and growth [28,31]. With the increase of the content of carbon nanotubes, the porosity gradually decreases, possibly due to the tubular structure of carbon nanotubes, Occupies the cross section of the aperture.

From Fig. 5, we can see that the trend of stress-strain curve of each support group is basically the same, and there are stress inflection points near the compression rate of 20% and 40%. Compared with these materials, after the strain value is 40%, the stress value under the same strain increases with the increase of carbon nanotube component content, and the size is 0.3% CNT >0.2% CNT >0.1% CNT >0% CNT. Through the stress-strain curve, we can then calculate the modulus of the corresponding sample and the compressive strength under the corresponding compression rate. Table 3 shows this information. It can be observed from the histogram in Fig. 6 that the young's modulus of the four composite scaffolds ranges from 40 to 80 MPa, and the modulus level is very close to human cancellous bone (Young's modulus is 50 MPa) [32]. Such mechanical strength is close to human cartilage tissue, so that the composite scaffolds can meet the mechanical requirements of cartilage tissue. It can be observed in Figs. 1–9 that the change trend of compression strength with compression ratio of 80% is consistent with that of compression modulus.

3.3. Systemic toxicity test

There was no death, irritability, salivation and convulsion poisoning in the experimental group and the control group within 1D, 2D

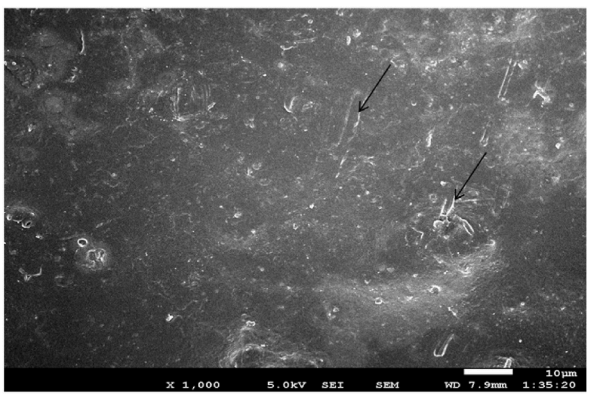

Fig. 3. Shows PCL under electron microscope/β- Microstructure of TCP/CNT composite scaffold (×1000). Note: a large number of carbon nanotubes can be seen in the figure in tubular structure and white granules β- Tricalcium phosphate is evenly dispersed in polycaprolactone (arrow).

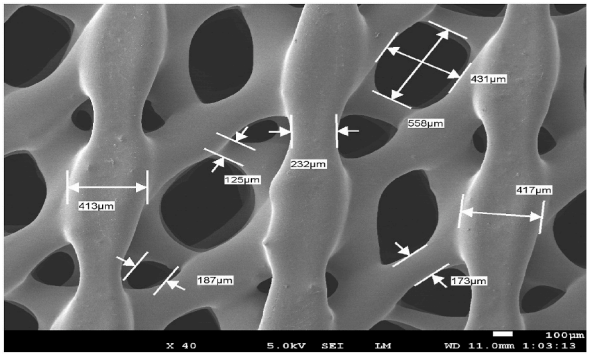

Fig. 4. Shows the measurement of microstructure and dimension of composite support (× 40). Note: PCL is listed in the figure/β- According to the measurement data of TCP/0.2% CNT stent group, the fiber diameter was 374 ± 50.45 μm and the pore diameter of the stent was 396.2 ± 73.23 μm.

Table 3
Compressive strength, elastic modulus and porosity of composite supports in each group.

Compound material	Compressive strength (MPa)	Elastic modulus (MPa)	Support porosity (%)
PCL/β-TCP	27.94 ± 0.23	48.22 ± 0.32	65.07 ± 0.10%
PCL/β-TCP/0.1%CNT	30.54 ± 0.54	58.66 ± 0.35	62.36 ± 0.11%
PCL/β-TCP/0.2%CNT	34.00 ± 0.16	77.86 ± 0.52	62.02 ± 0.13%
PCL/β-TCP/0.3%CNT	42.72 ± 0.37	85.2 ± 0.68	60.42 ± 0.21%

Note: $P < 0.05$, with statistical difference.

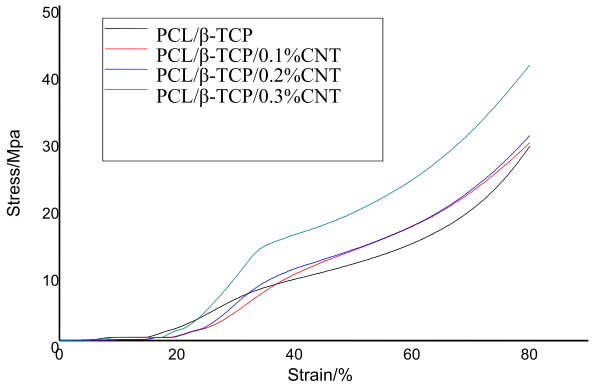

Fig. 5. Compressive stress-strain curve of each sample.

and 3D after injection. There were no abnormal activities, mental state, diet, sleep, hair and urine and stool in all rats. After 7 days, the experimental rats were killed, the liver and kidney organs were taken out, and no special changes in the size, color and blood supply of important organs were observed. The sections were stained with hematoxylin eosin, and the tissue sections were observed under the microscope. The microscopic manifestations of the experimental group and the control group were consistent (see Figs. 8–10). No abnormal acute toxic manifestations such as cell structure edema, necrosis and dissolution were found. In conclusion, it is proved that the scaffold material has good compatibility in animals, no obvious toxicity *in vivo*, and meets the requirements of biosafety materials (see Fig. 11).

3.4. Hemolysis test results

There was no hemolysis in each experimental group and negative control group (normal saline group), and obvious hemolysis occurred in positive control group (distilled water group) (see Fig. 12). The hemolysis rate results of composite scaffolds in this experiment are shown in Table 4 below. The hemolysis rate of four composite scaffolds is less than 5%, so the composite materials in this experiment meet the national biomaterial safety evaluation standard.

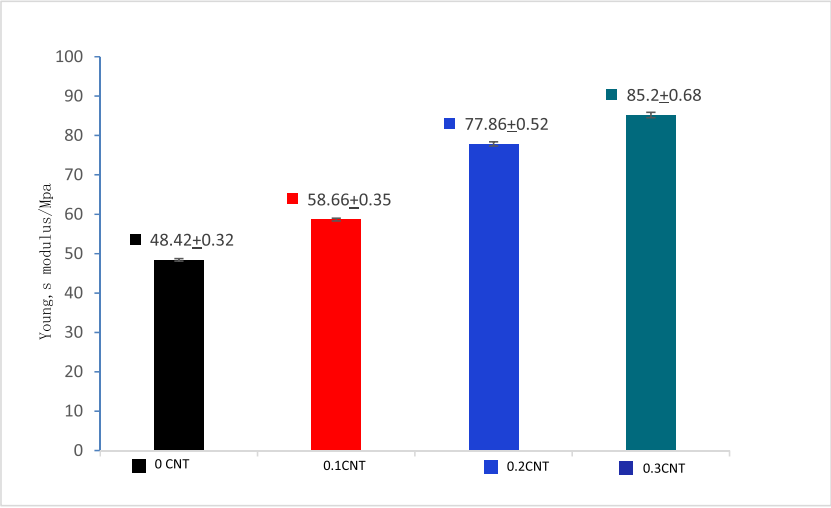

Fig. 6. Trend of elastic modulus of each sample.

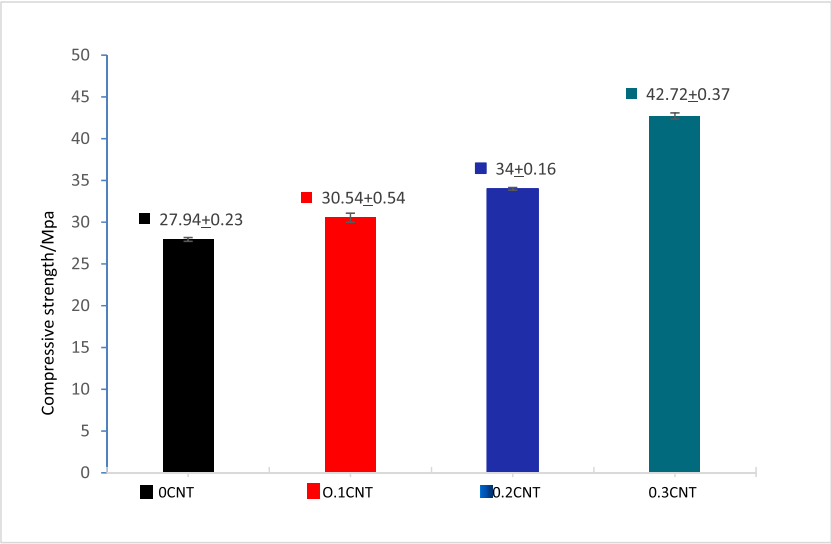

Fig. 7. Trend of compressive strength of each sample compressed to 80%.

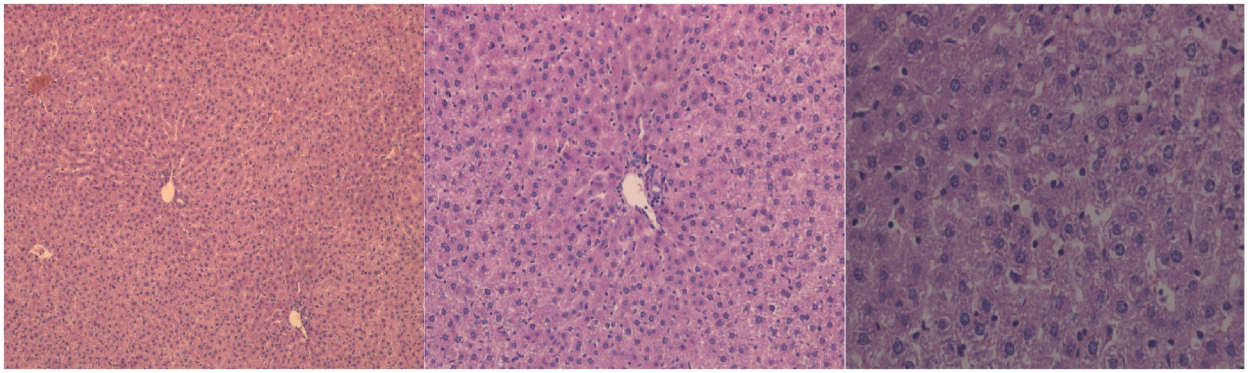

Fig. 8. Shows the liver tissues of rats in the experimental group at different magnification under the microscope (× 40 × 100 × 400) lower HE staining.

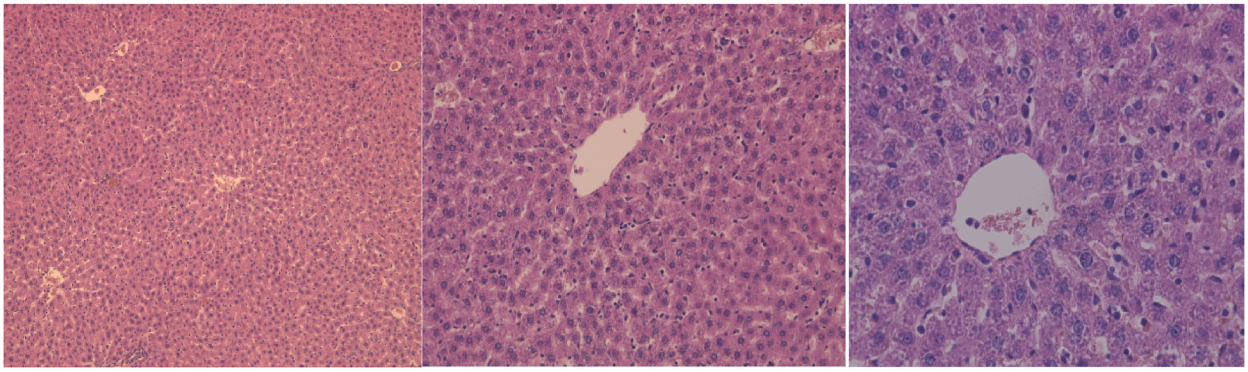

Fig. 9. Shows the liver tissues of rats in the control group at different magnification under the microscope (× 40 × 100 × 400) lower HE staining.

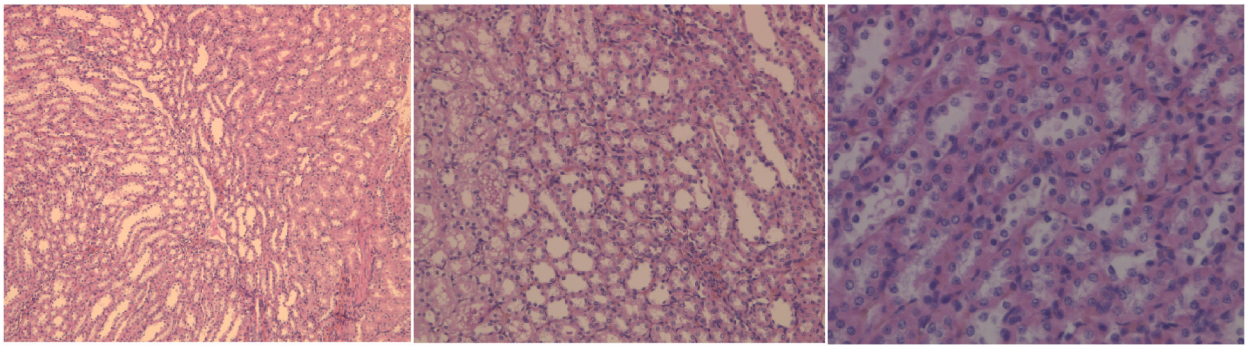

Fig. 10. Shows the renal tissues of rats in the experimental group at different magnification under the microscope (×40 × 100 × 400) lower HE staining.

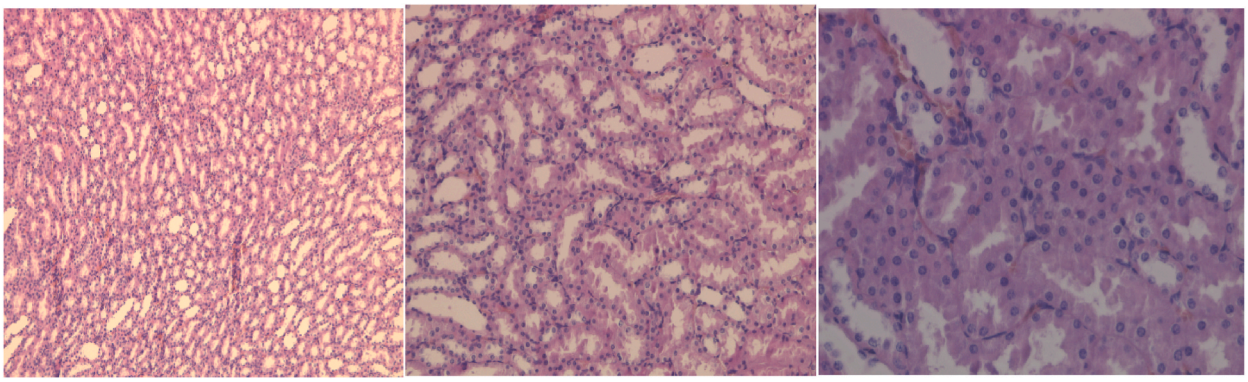

Fig. 11. Shows the renal tissues of rats in the control group at different magnification under the microscope (× 40 × 100 × 400) lower HE staining.

3.5. Morphological observation and analysis of ADSC

The cells were continuously observed under an inverted microscope. The newly extracted primary ADSCs were suspended in the culture medium in a round or oval shape (Fig. 13a). After 12 h, some cells adhered to the wall. At the initial stage, the cells were small in volume, spindle or spindle shape, arranged and distributed disorderly (Fig. 13b). After 7 days, the cell volume increased, the morphology was similar to fibroblasts, spindle shaped, uniform adhesion and abundant cytoplasm, The nucleus is large and centered, the nucleolar nuclear membrane is clear, the glial secretion around the cell is strong, and the refraction is strong (Fig. 13C). When the cells were cultured to 90% confluence, they were subcultured according to the ratio of 1:2. After subculture to the third generation (Fig. 13d), the cells proliferated in large numbers, were spindle shaped, adhered evenly to the wall, and the local collection was whirlpool or parallel and closely arranged.

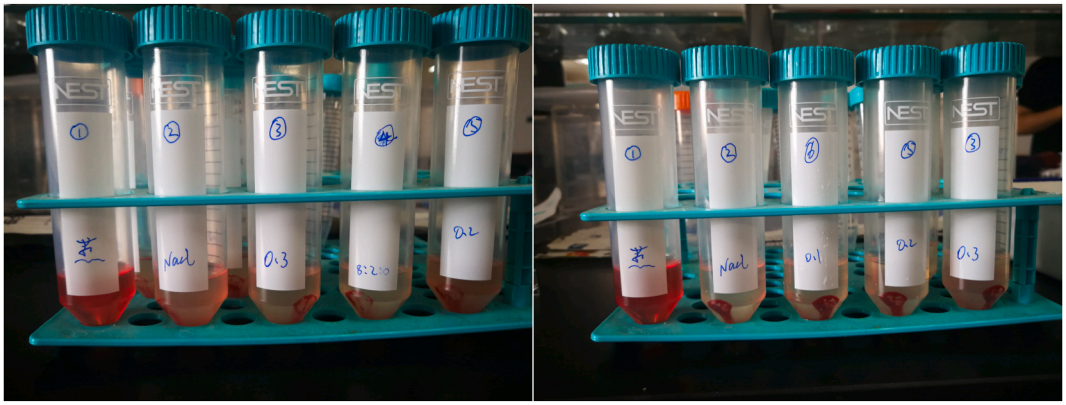

Fig. 12. Shows the hemolysis test results of four composite scaffolds. Note: tube 1 is the hemolysis test of distilled water in the positive control group. Hemolysis is positive and the liquid is light red; Tube 2 is the hemolysis test of normal saline in the negative control group, no obvious hemolysis is found, and the color of the solution has no obvious change. 3. Pipe 4, 5 and 6 are PCL respectively/β- TCP/0.3%CNT、PCL/β- TCP、PCL/β- TCP/0.2%CNT、PCL/β- In the hemolysis test of the extract of TCP/0.1% CNT composite scaffold, no obvious hemolysis was found, and the color of the solution did not change significantly. (For interpretation of the references to color in this figure legend, the reader is referred to the Web version of this article.)

Table 4
A value of each group and hemolysis rate of each experimental group.

Group	Absorbance value of each tube			Mean value	Hemolysis rate
	1	2	3		
PCL/β-TCP/0.3%CNT	0.127	0.127	0.129	0.128 ± 0.001	1.937%
PCL/β-TCP/0.2%CNT	0.131	0.131	0.129	0.130 ± 0.001	2.290%
PCL/β-TCP/0.1%CNT	0.121	0.125	0.120	0.122 ± 0.003	1.189%
PCL/β-TCP	0.125	0.128	0.123	0.125 ± 0.003	1.629%
Negative control group	0.114	0.115	0.110	0.113 ± 0.003	
Positive control group	0.850	0.885	0.876	0.870 ± 0.018	

Note: $P < 0.05$, with statistical difference.

3.6. *Effect of composite scaffold on ADSC proliferation*

The OD value of cells in each group was detected by CCK-8 method, which clearly reflected the effect of scaffolds in each group on ADSC proliferation. With the growth of culture time, ADSC cells in the scaffold extraction culture medium in each group were also proliferating (see Fig. 14). On days 2, 4 and 6, different proportions of PCL/β- Compared with PCL, TCP/CNT stent group/β- TCP stent group had the effect of promoting ADSC proliferation ($P < 0.05$), and PCL/β- The OD value of TCP/0.2% CNT scaffold group was significantly higher than that of other experimental groups ($P < 0.05$), and the significance of the difference was obvious with the increase of culture time (Table 5).

4. Discussion

It is well known that bone tissue has the ability of self-regeneration, but the body can not completely cure large-area bone defects. In most cases, external intervention is needed to restore and help bone healing [33,34]. The adaptive function of bone tissue structure includes many levels, including: the molecular structure and distribution of crystal and organic components; Structure of bone plate; the structure and arrangement of spongy bone tissue and dense bone tissue; Macrostructure [35,36], therefore, the development of appropriate three-dimensional scaffolds is very important to construct functionally equivalent bone tissue.

Four basic categories of scaffold properties can be modified, enhanced, or altered to make a scaffold appropriate for bone tissue engineering applications: [a] biological necessities, [b] anatomical characteristics, and [c] biomaterial composition and [d] bio-fabrication techniques. Generally, the scaffold needs to be non-toxic and biocompatible first and foremost. Specifically, cells need to adhere, perform correctly, multiply, differentiate, and produce new matrix for physiological performance. The bio-resorbale and biodegradable properties of the scaffolds has the capacity to induce tissue synthesis while degradation of the biomaterial. Novel biomaterials that more closely resemble the 3D bone structure in terms of mechanical characteristics as well as osteo-inductive, osteo-conductive, and osteo-genic qualities have been developed as a result of recent advancements in bone tissue engineering. The scaffold should be made up of composites as the bone is non-homogenous. So that it can mimic the native structure of bone. This is why the scaffold was fabricated with various layers of materials and composites [37].

3D printing or Rapid Prototyping (RP) is a recent bio fabrication method for developing the scaffolds for tissue engineering. These

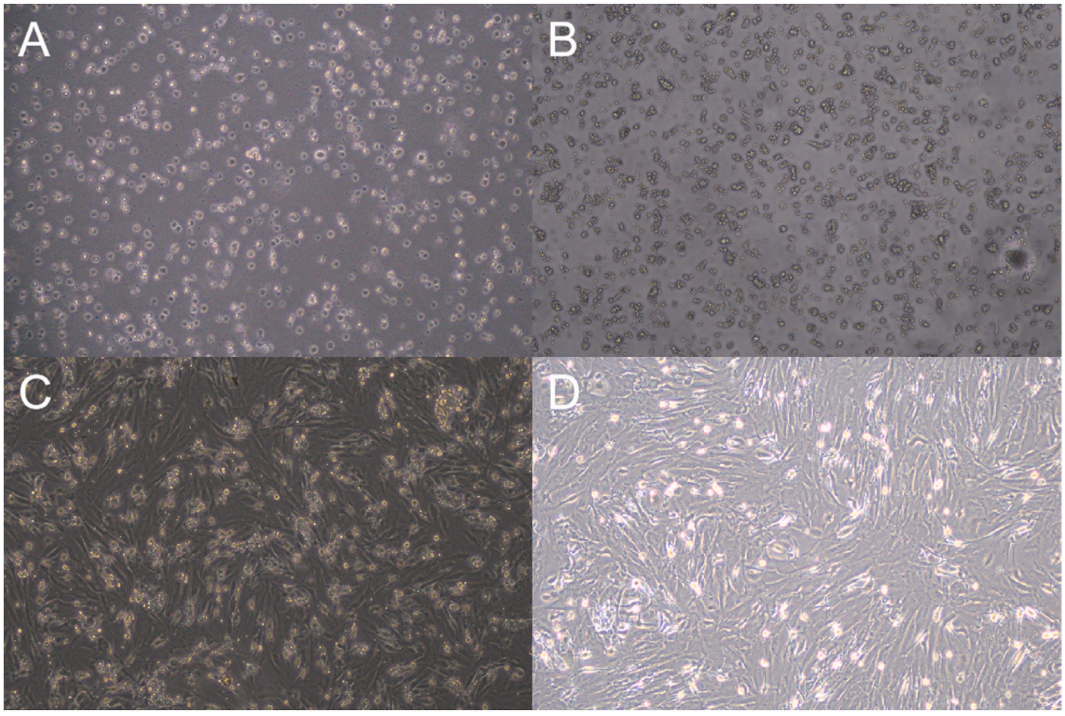

Fig. 13. Shows the cell morphology (100x) of rat adipose stem cells (ADSC) at different stages Note: Fig. 13A shows the state of primary ADSC just inoculated, and the cell suspension is round or oval; Fig. 13b shows the state of primary ADSC inoculated seeds cultured for 12 h. Some cells adhered to the wall and grew in spindle or spindle shape; Fig. 13C cell state of primary ADSC when inoculated and cultured for 7 days, the cells adhered to the wall and grew in spindle shape; Fig. 13d shows the cell state of the third generation ADSC cultured for 5 days. The cells adhered to the wall and grew in a spindle shape.

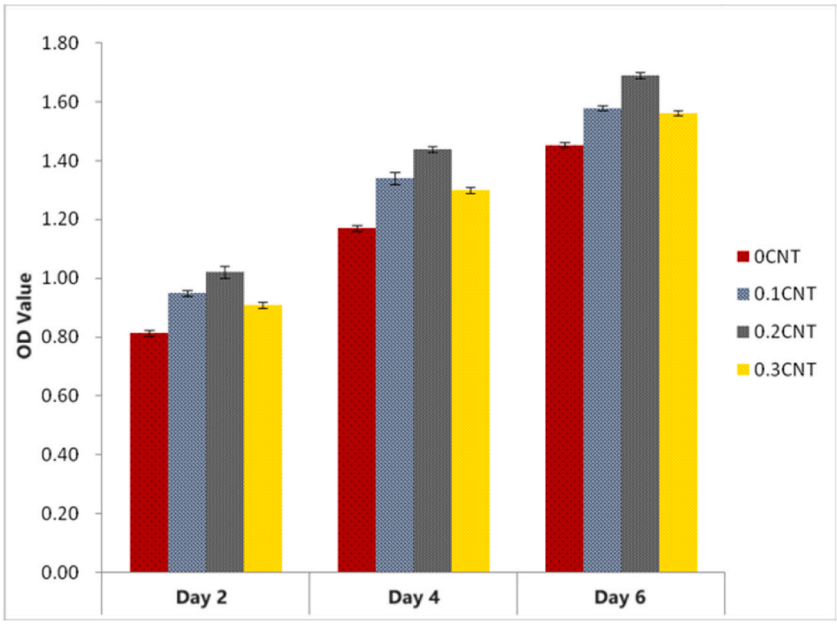

Fig. 14. Test results of proliferation activity of ADSC cultured in four composite scaffold extracts for one week. Note: the proliferative activity of adipose stem cells cultured in different scaffold material extracts and culture media is polycaprolactone/β- Tricalcium phosphate/0.2% carbon nanotube scaffold > polycaprolactone/β- Tricalcium phosphate/0.1% carbon nanotube scaffold > polycaprolactone/β- Tricalcium phosphate/0.3% carbon nanotube scaffold > polycaprolactone/β- Tricalcium phosphate scaffold ($P < 0.05$).

Table 5
Statistical analysis of ADSC proliferation results on scaffold materials of each group at different time points (OD value: X ± s, n = 9).

Bracket group	TIME		
	Day 2	Day 4	Day 6
PCL/β-TCP	0.81 ± 0.01	1.17 ± 0.01	1.45 ± 0.01
PCL/β-TCP/0.1%CNT	0.95 ± 0.01	1.34 ± 0.02	1.58 ± 0.01
PCL/β-TCP/0.2%CNT	1.02 ± 0.02	1.44 ± 0.01	1.69 ± 0.01
PCL/β-TCP/0.3%CNT	0.91 ± 0.01	1.30 ± 0.01	1.56 ± 0.01
F	215.681	284.855	357.700
P	0.000	0.000	0.000

Note: $P < 0.05$, with statistical difference.

methods generally avoid using hazardous organic solvents, which greatly improves the scaffold's biocompatibility. It is able to tailor porosity, pore size, mechanical, and chemical properties very precisely, which makes it possible to replicate the structure of real bone tissue more accurately. The bulk, interface, and surface of the scaffold can all have different material compositions thanks to these techniques. The foundation of RP technology is the ability to create objects (CAM) from the description of a 3D mathematical model (CAD). Three parts make up CAD/CAM systems: a digitalization tool/scanner that converts geometry into computer-processable digital data; software that creates a data set that a fabrication machine can read; and manufacturing technology that turns the data set into the intended product [37].

Among the most advanced technologies available, the combination of rapid prototyping (RP) or three-dimensional (3D) printing technology with computer-aided design (CAD) and computer-aided manufacturing (CAM) is the most effective strategy to replicate complex bone anatomy to develop patient specific grafts [38]. As we discussed earlier, these three-dimensional bone scaffolds must meet the specific requirements of bone tissue growth, such as biocompatibility, bone conductivity, appropriate pore size structure, bone integration, biodegradability and bio-absorption. In addition, they should have compatible mechanical properties (similar to bones) and simple processing [39,40]· To achieve the above conditions, a suitable pore structure must be designed, which allows stable mechanical, bone cell migration, adhesion and proliferation in order to heal the injured tissue [23,41].

In 3D Printing process, the Fusion-Deposition Modeling (FDM) process involves depositing molten thermoplastic materials onto a base platform, followed by a path defined by CAD and CAM. 3D scaffolds with controllable pore size and porosity can be fabricated by changing material deposition amount, spacing between material paths, and height interval. The main advantages of FDM are material high porosity, good mechanical strength, no toxic solvent requirement, and flexibility in material handling and processing. FDM can also be used to produce composites like PCL-HA or PCL-TCP, used in bone thinning (BTE) for their mechanical and biochemical properties. However, the main difficulty is the requirement for preformed fibers with consistent size and material properties to feed through rollers and nozzles. Modified FDM processes have been developed to overcome these issues [37].

In this investigation, FDM technology in 3D printing is used to successfully print the pre-defined personalized solid support with the help of CAD software. FDM technology is the earliest printing technology based on extruded molten polymer. Its printing process has the characteristics of high precision, high efficiency, low cost and strong repeatability.

PCL is thermoplastic and linear aliphatic polyester that is commonly utilized in the production of bone scaffolds in tissue engineering practices. This semi-crystalline polymer is appropriate for use in load-bearing bones because of its high biocompatibility, low cost, simple processing, non-carcinogenicity, low immunogenicity, and slow degradation rate. By combining PCL with growth factors, medications, cells, and other biomaterials, its qualities have been enhanced and bone lesions have been assisted in healing. The new 3D printing technique, when combined with PCL composites, offers a promising new avenue for the successful treatment of bone injuries [42]. More than a few decades ago, PCL-based scaffolds were first used for BTE and these scaffolds implanted, and assisted in the repair of bone defects. As previously stated, PCL is an aliphatic polyester and linear thermoplastic that has received approval from the Food and Drug Administration (FDA). There is enough promise for this semi-crystalline polymer to be used in high-load bearing bones [42].

Ceramics are typically brittle, hard, oxidation-, wear-, and thermal-resistant materials with low tensile strength and high compression strength. Compared to pure PCL, PCL/ceramic composite materials have better mechanical qualities, bioactivity, hydrophilicity, and biodegradability. The most often used ceramic materials in combination with PCL are hydroxyapatite, carbon nanotubes (CNTs), β-tricalcium phosphate (β-TCP), graphene, and mesoporous bioactive glasses [42].

As polycaprolactone (PCL) is the matrix material of the composite support, its content is large and its viscosity is high, so we choose the barrel feeding mode to directly heat and melt the block material, so as to avoid blocking the nozzle. Polycaprolactone has the characteristics of low melting point, which makes it easier to composite with other biomaterials. The composite material does not affect the excellent characteristics of polycaprolactone such as thermal stability, biodegradability and plasticity [11,43], which is also one of the reasons for its wide application. In order to endow scaffolds with bone induction and bone conduction characteristics, PCL is often mixed with bioceramics, such as hydroxyapatite (HAP), β- Tricalcium phosphate (β-TCP) and biphasic calcium phosphate (BCP) [44]. β- TCP is mainly composed of calcium and phosphorus, which is similar to the inorganic components of bone matrix, and it combines well with bone. Due to its excellent biocompatibility, *in vivo* absorbability and good osteo-conductivity, TCP is widely studied and used as a transplantable biomaterial for bone repair [45]. A large number of studies have confirmed PCL/β- TCP composite scaffold has good performance [46]. But now based on β- Porous scaffolds of TCP often encounter inherent and uncontrolled brittleness, which hinders their application, especially as load-bearing implants for bone regeneration [21]. However, due to its good mechanical strength [47], CNT can manufacture carbon nanotube composites with mechanical properties matching with bones, which

can improve PCL/β- Mechanical strength of TCP.

Research findings indicate that the incorporation of β-TCP, an osteo-conductive material, into PCL enhanced its mechanical strength, biodegradability, and ability to bind to proteins, growth factors, and cells in the resultant composite. Bone tissue can enter the resulting composite due to the double holes on the TCP surfaces. It was investigated that the incorporation of β-TCP could enhance the bone scaffold's mechanical characteristics, biodegradability, and surface qualities. It was proved that the incorporation of β-TCP could enhance the bone scaffold's mechanical characteristics, biodegradability, and surface qualities. When combined with PCL, CNTs—materials with well-established chemical, electrical, mechanical, and structural properties—improve the composite's electrical conductivity and promote bone healing. As imaging agents and carriers of bioactive molecules, carbon nanotubes are widely employed [48].

Most researchers believe that composite scaffolds should have appropriate pore size, which is conducive to bone cell growth and material transport. At the same time, the porosity of the scaffold is also a key factor affecting the osteogenesis effect. High porosity can make the composite scaffold lose the mechanical strength of the bone graft site, and the porosity is too low, which affects the material transport between the interior of the scaffold and between the interior of the scaffold and the external environment [28]. The composite scaffolds prepared this time were observed under scanning electron microscope that the internal pores were connected with each other, and the pore size was uniform. The measured pore size was 366.1 ± 57.47 μm-396.2 ± 73.23 μm, and the diameter of scaffold fiber was 351 ± 43.21 μm-377.4 ± 52.44 μm, which met the requirements of bone cell growth. The porosity of the scaffold is between 60.42 ± 0.21% - 65.07 ± 0.10%, which is consistent with the porosity of bone tissue engineering scaffold reported in previous studies (35%–75%). The porosity within this range is conducive to cell growth, material transport and tissue vascularization [32]. The research shows that the porosity and pore size of the scaffold have a certain impact on the mechanical properties of the material. Although the larger pore size may promote the nutrition and oxygen transfer between cells, the larger pore volume will also reduce the mechanical properties of the scaffold [29]. The mechanical strength of bone tissue engineering scaffold is related to the supporting function of the scaffold in the load-bearing part. Therefore, selecting high mechanical strength materials to construct scaffolds is a great solution to balance mechanical strength with porosity and pore size.

Through the comparison with the 3D printed scaffolds of these categories in scientific literatures, as it was reported on the pore size of 3D Printed scaffolds without calcium phosphate particles, the average pore size is roughly 1.16 ± 0.05 mm, but in scaffolds containing particles, the average pore size is 1.36 ± 0.01 mm. The scaffolds without particles have pore walls that measure roughly 0.72 ± 0.13 mm, whereas the scaffolds that incorporate particles have walls that measure 0.78 ± 0.03 mm. The presence of particles in the filament is likely the cause of the variations in porosity between the two types of 3D Printed scaffolds. Because the calcium phosphate particles prevent the polymeric material from recovering elastically, they cause the PCL filament's surface to become rougher, giving it some stiffness. This stiffness shows up as a few minor variations in the pore sizes of the particulate scaffolds. The manufactured filament's varied diameter may be the cause of the pore size variation, which could result in an uneven extrusion width and misalignment of the continuously deposited fibers during 3D printing. Scaffolds typically have pore diameters between 100 and 100,000 μm to promote vascularization and the development of new tissue [49].

In the present investigation, with the gradual increase of CNT content, the elastic modulus of the corresponding scaffold is also increasing. The young's modulus ranges from 48.22 ± 0.32 to 85.2 ± 0.68 MPa, and the modulus level is composite with the level of human cancellous bone (Young's modulus is 50 MPa) [33]. It was also reported that 3D Printed pure PCL Scaffold's Young's modulus was 0.35 GPa. Here, the composites' Young's modulus ranges from 0.05–0.1 GPa to 3–30 GPa. This is in the range of the cancellous bone. The use of these composite scaffolds for bone tissue engineering applications is further supported by our results [50]. Such mechanical strength is close to that of human cartilage tissue, so that the composite scaffold can match with human bone, So as to avoid the stress shielding effect at the implantation site.

The mechanical properties of 3D Printed PCL pure and 80/20 PCL + HA scaffolds was reported to be mean values of 3.2 MPa and 4.2 MPa for compressive strength and 44.1 MPa and 72.1 MPa for compressive modulus, respectively. The outcomes demonstrated that the compressive strength of scaffolds was unaffected by the addition of CP (Calcium phosphate) particles to the PLC volume. Nonetheless, there may be a slight trend toward an increase in the Young modulus [49].

The young's modulus of the PCL-CNT-5% composite prepared via FDM -3D printing was reported to be mean value of 0.87 ± 0.10 GPa. The modulus of the pure PCL 3D printed scaffold was found to be 0.51 ± 0.18 GPa confirming that the incorporation of CNT into PCL shows 70% improvement in E-Modulus than pure PCL scaffolds. In comparison to PCL, PCL-CNT-1 and PCL-CNT-3 likewise exhibit improvements in the E value of 35% and 55%, respectively. The average E values of PCL-CNT-1% and PCL-CNT-3% are 0.69 ± 0.15 and 0.79 ± 0.06 GPa, in that order. Compared to PCL-CNT-1 and PCL-CNT-3, the average E value of PCL-CNT-5 nanocomposite is marginally higher. In addition to that, the incorporation of CNT into PCL increase the hardness of the scaffolds. The increasing content of CNT reinforcement in the PCL matrix explains the observed increase in hardness. With an increase in CNT content, the elastic modulus, peak load value, and hardness all rise [51]. In addition to that, the incorporation of CNT into PCL increase the hardness of the scaffolds. The increasing content of CNT reinforcement in the PCL matrix explains the observed increase in hardness. With an increase in CNT content, the elastic modulus, peak load value, and hardness all rise [51].

In this study, the printed composite scaffolds were also tested for systemic toxicity and hemolysis rate, and the results met the national medical device evaluation standards. At the same time, through the detection of the proliferation activity of ADSC in the extract and culture medium of each group of materials, it can be found that polycaprolactone doped with 0.2% concentration of carbon nanotubes/β- Tricalcium phosphate scaffold can promote the growth of ADSC cultured in vitro, and the promoting effect is significantly higher than that of other groups.

The incorporation of CNT in the PCL scaffold enhances the proliferation of the cells on the scaffolds than that of Pure PCL scaffolds. Over the course of four days, the MTT assay assessed the toxicity and viability of H9c2 mouse myoblast cells on PCL and its

nanocomposite scaffolds. The outcomes demonstrated that both PCL and PCL-CNT nanocomposite scaffolds supported viable cell growth, with PCL-CNT-1 scaffold exhibiting higher proliferation than PCL or PCL-CNT-3 scaffolds. The fact that there was no discernible variation between the control and the scaffolds, however, suggests that the scaffolds might offer better adhesion and proliferation conditions. All scaffolds exhibited cell proliferation, but PCL-CNT-1 displayed greater growth [51].

With hBMSCs, PCL/TCP is biocompatible. In addition to encouraging hBMSC proliferation, it aids in the differentiation of reparative hard tissue. For hard tissue repair applications, 3D printed beta-TCP bio composites containing 50% (weight) PCL as the optimal option. TCP bio-ceramics break down rather quickly and encourage the growth of new bone *in vivo*. When creating a new material, biodegradation is essential; the rate of degradation must facilitate and expedite tissue regeneration.30 Furthermore, because osteoblasts prefer hydrophilic surfaces, the hydrophilic qualities of biomaterials for bone replacement are crucial for inducing early cell attachment and growth. This has also been seen in biocomposites, where composites with increased cell adhesion are produced by decreasing the contact angle. Given its substantial impact on the adhesion, proliferation, and differentiation of hBMSCs, surface wettability is an important factor that needs to be taken into account [52].

Comparing the mesenchymal stromal cells (MSCs) cultured in the 3D printed PCL/TCP scaffold to the control group, there was an increase in osteogenic differentiation. MSCs grown on the 3D printed PCL/TCP scaffold exhibited less osteogenic differentiation activity than cells grown on the scaffold in bone differentiation medium. All of these findings suggest that the PCL/TCP scaffold, which was printed three times, encouraged MSCs to differentiate into osteogenic tissue and may find extensive application in bone tissue engineering [53].

PCL biomaterials has the potential of subjected to fusion deposition modeling (FDM)_ and has less thermal degradation [54]. When PCL is mixed or copolymerized with additional materials, the scaffold's mechanical, surface, and physicochemical properties change. Accordingly, a number of studies have combined PCL with other metals, ceramics, and polymers to enhance its properties [48]. It was proved that the incorporation of β-TCP might enhance the bone scaffold's mechanical characteristics, biodegradability, and surface qualities [48]. Therefore, polycaprolactone/β- Tricalcium phosphate/0.2% carbon nanotube scaffold are expected to be a substitute for bone defect repair. At the same time, for the future construction of polycaprolactone/β-TCP. It provides a theoretical basis for the feasibility of tricalcium phosphate/carbon nanotube composite scaffold in the treatment of bone defect in animal model experiment.

5. Conclusion

The study investigated the fabrication of a polycaprolactone/β-Tri-calcium phosphate (TCP) scaffold with carbon nanotube (CNT) using 3D printing technology. The composite material was tested for mechanical strength, porosity, toxicity, hemolysis rate, and proliferation of rat adipose derived stem cells (ADSC). The composite scaffold, designed with CAD software and 3D printing, showed a high porosity, non-toxic, and non-hemolytic properties. The results showed that the polycaprolactone/β-tricalcium phosphate/0.2% carbon nanotube scaffolds had more advantages in promoting ADSC proliferation. The combination of 3D printing technology and CAD software allows for personalized composite stents with repeatability, high precision, and low cost. The scaffold's biocompatibility and strength make it a promising tool for bone tissue engineering applications.

Declaration

Experimental animal: Wistar rats, 10 week old female (Beijing weitonglihua Experimental Animal Technology Co., Ltd., license No.: scxk (Jing 2016–0006), Certificate No.: 1100111911053155). It has been confirmed that the study complies with all regulations.

Data availability

All data generated or analysed during this study are included in this published article; the raw datasets generated during and/or analysed during the current study are not available in the public repository. It can be provided based on the reasonable request to corresponding author.

CRediT authorship contribution statement

Yuelei Wang: Writing – review & editing, Writing – original draft, Methodology, Conceptualization. **Chenjing Liu:** Writing – review & editing, Writing – original draft, Validation, Methodology, Formal analysis, Conceptualization. **Tao Song:** Writing – review & editing, Data curation. **Zhenlu Cao:** Writing – review & editing, Validation, Formal analysis, Data curation. **Ting Wang:** Writing – review & editing, Supervision, Resources, Project administration, Funding acquisition.

Declaration of competing interest

.

References

[1] G.F. Rogers, A.K. Greene, Autogenous bone graft: basic science and clinical implications, J. Craniofac. Surg. 23 (1) (2012) 323–327.

[2] V. Campana, G. Milano, E. Pagano, M. Barba, C. Cicione, G. Salonna, W. Lattanzi, G. Logroscino, Bone substitutes in orthopaedic surgery: from basic science to clinical practice, J. Mater. Sci. Mater. Med. 25 (10) (2014) 2445–2461.
[3] S. Bose, M. Roy, A. Bandyopadhyay, Recent advances in bone tissue engineering scaffolds, Trends Biotechnol. 30 (10) (2012) 546–554.
[4] F.M. Najafabadi, S. Karbasi, S.Z. Benisi, S. Shojaei, S.A. Poursamar, R.N. Azadani, Evaluation of the effects of alumina nanowire on 3D printed polycaprolactone/magnetic mesoporous bioactive glass scaffold for bone tissue engineering applications, Mater. Chem. Phys. 303 (2023) 127616.
[5] Z. Ortega, M.E. Alemán, R. Donate, Nanofibers and microfibers for osteochondral tissue engineering, in: J. Oliveira, S. Pina, R. Reis, J. San Roman (Eds.), Osteochondral Tissue Engineering, Advances in Experimental Medicine and Biology, vol. 1058, Springer, Cham, 2018, https://doi.org/10.1007/978-3-319-76711-6_5.
[6] T. Garg, A.K. Goyal, Biomaterial-based scaffolds–current status and future directions, Expet Opin. Drug Deliv. 11 (5) (2014) 767–789.
[7] R. Agarwal, A.J. García, Biomaterial strategies for engineering implants for enhanced osseointegration and bone repair, Adv. Drug Deliv. Rev. 94 (2015) 53–62.
[8] F.M. Najafabadi, S. Karbasi, S.Z. Benisi, S. Shojaei, Physical, mechanical, and biological performance of chitosan-based nanocomposite coating deposited on the polycaprolactone-based 3D printed scaffold: potential application in bone tissue engineering, Int. J. Biol. Macromol. (2023) 125218.
[9] T.H. Qazi, D.J. Mooney, M. Pumberger, S. Geissler, G.N. Duda, Biomaterials based strategies for skeletal muscle tissue engineering: existing technologies and future trends, Biomaterials 53 (2015) 502–521.
[10] M.J. Mondrinos, R. Dembzynski, L. Lu, V.K. Byrapogu, D.M. Wootton, P.I. Lelkes, J. Zhou, Porogen-based solid freeform fabrication of polycaprolactone-calcium phosphate scaffolds for tissue engineering, Biomaterials 27 (25) (2006) 4399–4408.
[11] P. Sawadkar, J. Mohanakrishnan, P. Rajasekar, B. Rahmani, N. Kohli, L. Bozec, E. García-Gareta, A synergistic relationship between polycaprolactone and natural polymers enhances the physical properties and biological activity of scaffolds, ACS Appl. Mater. Interfaces 12 (12) (2020) 13587–13597.
[12] O. Janoušková, Synthetic polymer scaffolds for soft tissue engineering, Physiol. Res. 67 (Suppl 2) (2018) S335–s348.
[13] Q. Liu, L. Cen, S. Yin, L. Chen, G. Liu, J. Chang, L. Cui, A comparative study of proliferation and osteogenic differentiation of adipose-derived stem cells on akermanite and beta-TCP ceramics, Biomaterials 29 (36) (2008) 4792–4799.
[14] Y. Takahashi, M. Yamamoto, Y. Tabata, Osteogenic differentiation of mesenchymal stem cells in biodegradable sponges composed of gelatin and beta-tricalcium phosphate, Biomaterials 26 (17) (2005) 3587–3596.
[15] S.D. McCullen, Y. Zhu, S.H. Bernacki, R.J. Narayan, B. Pourdeyhimi, R.E. Gorga, E.G. Loboa, Electrospun composite poly(L-lactic acid)/tricalcium phosphate scaffolds induce proliferation and osteogenic differentiation of human adipose-derived stem cells, Biomed. Mater. 4 (3) (2009) 035002.
[16] Janset Oztemur, Suzan Ozdemir, Havva Tezcan-Unlu, Gulsah Cecener, Hande Sezgin, Ipek Yalcin-Enis, Investigation of biodegradability and cellular activity of PCL/PLA and PCL/PLLA electrospun webs for tissue engineering applications, Biopolymers 114 (2023) 11, https://doi.org/10.1002/bip.23564.
[17] Y.S. Zhang, K. Yue, J. Aleman, K. Mollazadeh-Moghaddam, S.M. Bakht, J. Yang, A. Khademhosseini, 3D bioprinting for tissue and organ fabrication, Ann. Biomed. Eng. 45 (2017) 148–163.
[18] E.H. Backes, S.V. Harb, C.A.G. Beatrice, K.M.B. Shimomura, F.R. Passador, L.C. Costa, L.A. Pessan, Polycaprolactone usage in additive manufacturing strategies for tissue engineering applications: a review, J. Biomed. Mater. Res. B Appl. Biomater. 110 (6) (2022) 1479–1503.
[19] M. Nikbakht, S. Karbasi, S.M. Rezayat, S. Tavakol, E. Sharifi, Evaluation of the effects of hyaluronic acid on poly (3-hydroxybutyrate)/chitosan/carbon nanotubes electrospun scaffold: structure and mechanical properties, Polymer-Plastics Technology and Materials 58 (18) (2019) 2031–2040.
[20] S. Shahi, S. Karbasi, T. Ahmadi, F. Naeimi, V. Goodarzi, S. Ebrahimi-Barough, Evaluation of physical, mechanical and biological properties of β-tri-calcium phosphate/Poly-3-hydroxybutyrate nano composite scaffold for bone tissue engineering application, Mater. Technol. 36 (4) (2021) 237–249.
[21] J. Zhang, W. Liu, V. Schnitzler, F. Tancret, J.M. Bouler, Calcium phosphate cements for bone substitution: chemistry, handling and mechanical properties, Acta Biomater. 10 (3) (2014) 1035–1049.
[22] R. Donate, M. Monzón, M.E. Alemán-Domínguez, Z. Ortega, Enzymatic degradation study of PLA-based composite scaffolds, Rev. Adv. Mater. Sci. 59 (1) (2020) 170–175.
[23] Y. Zhang, Y. Bai, B. Yan, Functionalized carbon nanotubes for potential medicinal applications, Drug Discov. Today 15 (11–12) (2010) 428–435.
[24] Y. Li, Z.G. Wu, X.K. Li, Z. Guo, S.H. Wu, Y.Q. Zhang, L. Shi, S.H. Teoh, Y.C. Liu, Z.Y. Zhang, A polycaprolactone-tricalcium phosphate composite scaffold as an autograft-free spinal fusion cage in a sheep model, Biomaterials 35 (22) (2014) 5647–5659.
[25] A. Yeo, C. Cheok, S.H. Teoh, Z.Y. Zhang, D. Buser, D.D. Bosshardt, Lateral ridge augmentation using a PCL-TCP scaffold in a clinically relevant but challenging micropig model, Clin. Oral Implants Res. 23 (12) (2012) 1322–1332.
[26] A. Khojasteh, H. Behnia, F.S. Hosseini, M.M. Dehghan, P. Abbasnia, F.M. Abbas, The effect of PCL-TCP scaffold loaded with mesenchymal stem cells on vertical bone augmentation in dog mandible: a preliminary report, Journal of biomedical materials research. Part B, Applied biomaterials 101 (5) (2013) 848–854.
[27] C.P. Firme 3rd, P.R. Bandaru, Toxicity issues in the application of carbon nanotubes to biological systems, Nanomed. Nanotechnol. Biol. Med. 6 (2) (2010) 245–256.
[28] Q.L. Loh, C. Choong, Three-dimensional scaffolds for tissue engineering applications: role of porosity and pore size, Tissue engineering, Part B, Reviews 19 (6) (2013) 485–502.
[29] V. Karageorgiou, D. Kaplan, Porosity of 3D biomaterial scaffolds and osteogenesis, Biomaterials 26 (27) (2005) 5474–5491.
[30] Influence of internal pore architecture on biological and mechanical properties of three-dimensional fiber deposited scaffolds for bone regeneration, J. Biomed. Mater. Res. 104 (8) (2016) 2108.
[31] M. Domingos, F. Intranuovo, A. Gloria, R. Gristina, L. Ambrosio, P.J. Bártolo, P. Favia, Improved osteoblast cell affinity on plasma-modified 3-D extruded PCL scaffolds, Acta Biomater. 9 (4) (2013) 5997–6005.
[32] S. Park, G. Kim, Y.C. Jeon, Y. Koh, W. Kim, 3D polycaprolactone scaffolds with controlled pore structure using a rapid prototyping system, J. Mater. Sci. Mater. Med. 20 (1) (2009) 229–234.
[33] R.C. Thomson, M.J. Yaszemski, J.M. Powers, A.G. Mikos, Fabrication of biodegradable polymer scaffolds to engineer trabecular bone, Journal of biomaterials science, Polymer edition 7 (1) (1995) 23–38.
[34] M. Navarro, A. Michiardi, O. Castaño, J.A. Planell, Biomaterials in orthopaedics, J. R. Soc., Interface 5 (27) (2008) 1137–1158.
[35] G.I. Im, Biomaterials in orthopaedics: the past and future with immune modulation, Biomater. Res. 24 (2020) 7.
[36] C. Gao, S. Peng, P. Feng, C. Shuai, Bone biomaterials and interactions with stem cells, Bone research 5 (2017) 17059.
[37] L. Roseti, V. Parisi, M. Petretta, C. Cavallo, G. Desando, I. Bartolotti, B. Grigolo, Scaffolds for bone tissue engineering: state of the art and new perspectives, Mater. Sci. Eng. C 78 (2017) 1246–1262.
[38] J.A. Robles-Linares, E. Ramírez-Cedillo, H.R. Siller, C.A. Rodríguez, J.I. Martínez-López, Parametric modeling of biomimetic cortical bone microstructure for additive manufacturing, Materials 12 (6) (2019).
[39] B. Yuan, S.Y. Zhou, X.S. Chen, Rapid prototyping technology and its application in bone tissue engineering, J. Zhejiang Univ. - Sci. B 18 (4) (2017) 303–315.
[40] K. Rezwan, Q.Z. Chen, J.J. Blaker, A.R. Boccaccini, Biodegradable and bioactive porous polymer/inorganic composite scaffolds for bone tissue engineering, Biomaterials 27 (18) (2006) 3413–3431.
[41] K.F. Leong, C.M. Cheah, C.K. Chua, Solid freeform fabrication of three-dimensional scaffolds for engineering replacement tissues and organs, Biomaterials 24 (13) (2003) 2363–2378.
[42] M. Gharibshahian, M. Salehi, N. Beheshtizadeh, M. Kamalabadi-Farahani, A. Atashi, M.-S. Nourbakhsh, M. Alizadeh, Recent advances on 3D-printed PCLbased composite scaffolds for bone tissue engineering, Front. Bioeng. Biotechnol. 11 (2023) 1168504.
[43] A. Butscher, M. Bohner, S. Hofmann, L. Gauckler, R. Müller, Structural and material approaches to bone tissue engineering in powder-based three-dimensional printing, Acta Biomater. 7 (3) (2011) 907–920.
[44] A. Bruyas, F. Lou, A.M. Stahl, M. Gardner, W. Maloney, S. Goodman, Y.P. Yang, Systematic characterization of 3D-printed PCL/β-TCP scaffolds for biomedical devices and bone tissue engineering: influence of composition and porosity, J. Mater. Res. 33 (14) (2018) 1948–1959.
[45] S.R. Motamedian, S. Hosseinpour, M.G. Ahsaie, A. Khojasteh, Smart scaffolds in bone tissue engineering: a systematic review of literature, World J. Stem Cell. 7 (3) (2015) 657–668.

[46] S.E. Kim, K. Park, Recent advances of biphasic calcium phosphate bioceramics for bone tissue regeneration, Adv. Exp. Med. Biol. 1250 (2020) 177–188.
[47] W. Wang, Y. Zhu, S. Liao, J. Li, Carbon nanotubes reinforced composites for biomedical applications, BioMed Res. Int. 2014 (2014) 518609.
[48] M. Gharibshahian, M. Salehi, N. Beheshtizadeh, M. Kamalabadi-Farahani, A. Atashi, M.-S. Nourbakhsh, M. Alizadeh, Recent advances on 3D-printed PCLbased composite scaffolds for bone tissue engineering, Front. Bioeng. Biotechnol. 11 (2023) 1168504.
[49] C. Garcia, Y. Orozco, A. Betancur, A.I. Moreno, K. Fuentes, A. Lopera, C. Paucar, Fabrication of polycaprolactone/calcium phosphates hybrid scaffolds impregnated with plant extracts using 3D printing for potential bone regeneration 9 (2) (2023).
[50] Shaun Eshraghi, Suman Das, Mechanical and microstructural properties of polycaprolactone scaffolds with one-dimensional, two-dimensional, and three-dimensional orthogonally oriented porous architectures produced by selective laser sintering, Acta Biomater. 6 (7) (2010) 2467–2476. ISSN 1742-7061.
[51] C.M.B. Ho, A. Mishra, P.T.P. Lin, S.H. Ng, W.Y. Yeong, Y.J. Kim, Y.J. Yoon, 3D printed polycaprolactone carbon nanotube composite scaffolds for cardiac tissue engineering, Macromol. Biosci. 17 (4) (2017) 1600250.
[52] S.H. Huang, T.T. Hsu, T.H. Huang, C.Y. Lin, M.Y. Shie, Fabrication and characterization of polycaprolactone and tricalcium phosphate composites for tissue engineering applications, J. Dent. Sci. 12 (1) (2017) 33–43.
[53] H. Park, J.S. Kim, E.J. Oh, T.J. Kim, H.M. Kim, J.H. Shim, W.S. Yoon, J.B. Huh, S.H. Moon, S.S. Kang, H.Y. Chung, Effects of three-dimensionally printed polycaprolactone/β-tricalcium phosphate scaffold on osteogenic differentiation of adipose tissue- and bone marrow-derived stem cells, Arch Craniofac Surg 19 (3) (2018 Sep) 181–189, https://doi.org/10.7181/acfs.2018.01879. Epub 2018 Sep 20. PMID: 30282427; PMCID: PMC6177683.
[54] Z. Ortega, M.E. Alemán, A.N. Benítez, M.D. Monzón, Theoretical–experimental evaluation of different biomaterials for parts obtaining by fused deposition modeling, Measurement 89 (2016) 137–144, https://doi.org/10.1016/j.measurement.2016.03.061. ISSN 0263-2241.